A Comparative QM/MM Simulation Study of the Reaction Mechanisms of Human and *Plasmodium falciparum* HG(X)PRTases

Aline Thomas* and Martin J. Field

Contribution from the Laboratoire de Dynamique Moléculaire, Institut de Biologie Structurale - Jean-Pierre Ebel (CEA/CNRS/UJF), 41 rue Jules Horowitz, 38027 Grenoble Cedex 1, France

Received February 3, 2006; E-mail: aline.thomas@ibs.fr

Abstract: QM/MM hybrid potential free-energy simulations are performed to compare the reaction mechanisms of human hypoxanthine guanine phosphoribosyl transferase (HGPRTase) and the corresponding enyzme from *Plasmodium falciparum* (*Pf*), hypoxanthine guanine xanthine phosphoribosyl transferase (HGXPRTase). These enzymes share 44% of sequence identity but display very different affinities for xanthine. The calculations show that in both enzymes phosphoribosyl transfer proceeds via a dissociative mechanism from an anionic form of the substrate. Nevertheless, there are significant differences in the geometries of critical structures along the reaction paths which it may be possible to exploit for the design of specific inhibitors against the *Pf* enzyme.

Introduction

Many parasitic protozoa overcome their inability to synthesize purines by scavenging these molecules from their hosts and transforming them into purine nucleotides. This process is carried out by purine phosphoribosyl transferase (PRTase) enzymes which, because they are essential to the parasites, represent potential therapeutic targets.[1-4] PRTases catalyze bond formation between the N9 atom of the imidazole ring of a purine base and the ribose C1′ atom of α-D-5-phosphoribosyl-1-pyrophosphate (PRPP). The overall reaction, shown in Scheme 1, is an ordered one with PRPP binding before the purine base and PPi (pyrophosphate) being released before the nucleotide.

In *Plasmodium falciparum* (*Pf*), which is the causative agent of malaria, the PRTase hypoxanthine-guanine-xanthine PRTase (HGXPRTase) processes the three purines, hypoxanthine, guanine, and xanthine, with similar efficiency. In contrast, the equivalent human enzyme, hypoxanthine-guanine PRTase (HGPRTase), shows a 100-fold reduced affinity for xanthine compared to hypoxanthine and guanine although it shares significant sequence identity (44%) with the *Pf* enzyme.[5] This difference in substrate selectivity has been addressed by the only other comparative theoretical study of these two enzymes.[6] In this work, Pitera et al. employed molecular dynamics techniques to conclude that the specificity difference arose from differences in the flexibility of the base-binding region of the active sites.

In the present paper we employed molecular modeling techniques with a hybrid quantum mechanical/molecular mechanical (QM/MM) potential to compare the reaction mechanisms of human and parasitic HG(X)PRTases. This is a follow-up to our earlier work on the *Pf* enzyme.[7,8] We wanted to investigate differences in the chemical steps of the mechanisms of the two enzymes with the aim of seeing whether this information could be useful for inhibitor design. Specific inhibitors need to be found, since a lack of human HGPRTase leads to severe diseases such as Lesch-Nyhan syndrome and gout.

Computational Details

Enzyme Model. Several PRTase crystal structures complexed to different ligands were used in this study. These are listed in Table 1. Of the three human PRTase crystal structure complexes, the 1BZY structure was taken as the starting enzyme model because of its higher resolution compared to 1HMP and its closed active-site configuration. However, to model the substrates hypoxanthine, xanthine, and PRPP in the active site, we employed the very high resolution 1FSG crystal structure as this is the only one which contains all the atoms implicated in the mechanism. In our previous studies of the *Pf* enzyme we used the 1CJB and 1FSG structures.[7,8]

The human and *Pf* enzymes share an overall 44% sequence identity, but this rises to 80% in the region of the active site (the sphere comprised within 10 Å of the C1′ atom). Likewise, the RMS coordinate deviation between the structures of the human and *Pf* enzymes is ~1.6 Å for the full protein but less than 0.5 Å for the active site only (superposition of Cα atoms only). A superposition of the crystal structure active sites of human and *Pf* enzymes bound with immucillin-type inhibitors is shown in Figure 1. Among the non-conserved residues in the active-site region, the substitution of $Arg169_{hum}$ for $Leu180_{Pf}$ is notable, since this residue hydrogen bonds to the catalytic aspartic acid, $Asp137_{hum}$ or $Asp148_{Pf}$.

Hybrid Potential Simulations. Our simulation study of the human enzyme used very similar procedures and techniques to those of our previous studies of the *Pf* enzyme,[7,8] and so only a brief description will be given here. We performed an extensive series of simulations

(1) Musick, W. D. L. *CRC Crit. Rev. Biochem.* **1981**, *X*, 1−34.
(2) Craig, S. P., III; Eakin A. E. *J. Biol. Chem.* **2000**, *275*, 20231−20234.
(3) Schramm, V. L.; Grubmeyer, C. *Prog. Nucleic Acid Res.* **2004**, *78*, 261−304.
(4) Schramm, V. L.; Shi, W. *Curr. Opin. Struct. Biol.* **2001**, *11*, 657−665.
(5) Xu, Y.; Grubmeyer, C. *Biochemistry* **1998**, *37*, 4114−4124.
(6) Pitera, J. W.; Munagala, N. R.; Wang, C. C. Kollman, P. A. *Biochemistry* **1999**, *38*, 10298−10306.
(7) Thomas, A.; Field, M. J. *J. Am. Chem. Soc.* **2002**, *124*, 12432−12438.
(8) Crehuet, R.; Thomas, A.; Field, M. J. *J. Mol. Graphics Modell.* **2005**, *24*, 102−110.

Scheme 1. Reaction Catalyzed by HG(X)PRTases[a]
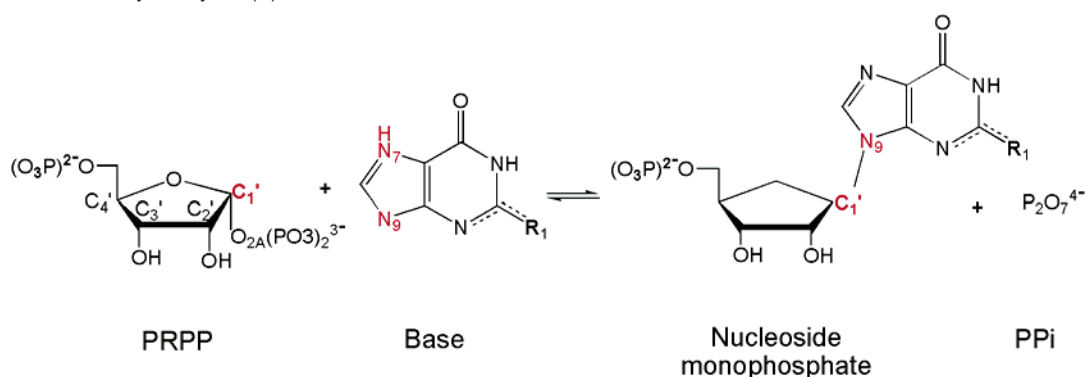
[a] R_1 = H, NH_2, and O for hypoxanthine, guanine, and xanthine, respectively. The corresponding products are inosine monophosphate (IMP), guanosine monophosphate (GMP), and xanthosine monophosphate (XMP).

with both the human and the *Pf* enzymes and with both hypoxanthine and xanthine as the reacting bases. Different initial conformations of the ribose substrate moiety were also tried as these are observed in the different crystal structures.

For our calculations of the reaction mechanism, we used semiempirical and ab initio QM/MM hybrid potentials. All simulations with hybrid potentials were performed with the Dynamo program,[14,15] whereas purely ab initio calculations were done with the Jaguar[16] program. As semiempirical methods we used the AM1[17] and PDDG/PM3[18] methods. The results with the two methods did not differ significantly for the phosphoribosyl transfer reaction, and so we only present the results obtained with the AM1 hybrid potentials. As ab initio methods we used Hartree−Fock (HF) and density functional theory (DFT) methods with the 6-31++G** basis set[19] and, for the DFT calculations, the B3LYP functional.[20] The OPLS-AA force field was used to represent the atoms in the MM region.[21]

The total simulation systems had approximately 21 000 atoms with between 50 and 100 atoms in the QM region. A schematic of the QM region is given in Figure 2. The smallest QM region we employed contained the base, PRPP and Asp 137. We studied this principally because we wanted to compare the AM1 and PDDG/PM3 methods, and the latter has not yet been parametrized for magnesium. The larger QM regions included the magnesiums and their ligands as well as Arg169 and Lys165. The AM1 magnesium parameters were taken from Hutter et al.[22] All covalent bonds between atoms belonging to the QM and MM regions were treated by the default link-atom methods in the Dynamo program. The method for semiempirical potentials is fully described in ref 15, whereas that for ab initio potentials corresponds to

model $LA_g(4,0)$ of ref 23. The methods are identical and differ only in the way in which the QM/MM electrostatic interactions are calculated for the QM link atoms and the MM boundary atoms (i.e., the MM atoms of the severed QM−MM covalent bonds). In the semiempirical method all QM/MM electrostatic interactions are included, except those for the QM link atoms. By contrast, all interactions, including those for the QM link atoms, are fully determined in the ab initio method but with the difference that the charge distributions of the MM boundary atoms are represented by Gaussians of a given width instead of delta functions.

The reaction path was modelled, as previously published,[7] using a mixture of constrained energy minimization, saddle-point and reaction-path location algorithms, and molecular dynamics simulations. The free-energy calculations were performed using the molecular dynamics method in conjunction with umbrella sampling. Two composite reaction coordinates, involving four interatomic distances, were found to give a good description of the reaction process. They were

$$\xi_1 = d[\text{N9}-\text{C1}'] - d[\text{C1}'-\text{O2A}]$$

and

$$\xi_2 = d[\text{H7}-\text{N7}] - d[\text{OD2(Asp137)}-\text{H7}].$$

ξ_1 and ξ_2 describe the phosphoribosyl and proton transfers, respectively. These coordinates are identical to those used for modeling the *Pf* enzyme reaction mechanism[7] thereby allowing a direct comparison to be made between the calculated free-energy surfaces of the human and *Pf* enzymes.

To calculate a reaction free-energy surface, a series of molecular dynamics simulations were performed in which ξ_1 and ξ_2 were constrained to have particular values using harmonic restraining potentials. ξ_1 was allowed to vary between −2.47 and 1.63 Å in increments of 0.07 Å, whereas ξ_2 varied between −0.97 and 0.94 Å in increments of 0.03 Å. The length of each simulation was 60 ps, of which the last 45 ps were used for construction of the free-energy surface using the WHAM methodology.[24,25] The generation of a full surface requires 3600 (60 × 60) simulations,[7] but in many cases, this is unnecessary as sampling a limited portion of the surface is sufficient for the identification of favorable pathways.

Transition states (TSs) were located using standard second derivative saddle-point location techniques and the QM(AM1)/MM(OPLS-AA) hybrid potential. Due to the expense of calculating and manipulating the second derivative matrix, only atoms within a 10 Å sphere of the ribose C1′ atom were optimized in these calculations. Normal-mode
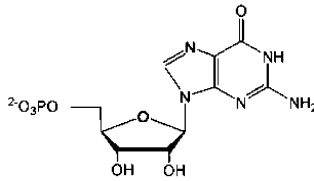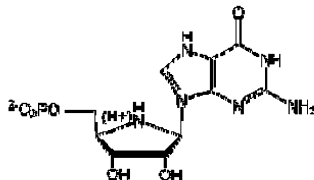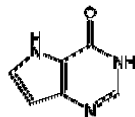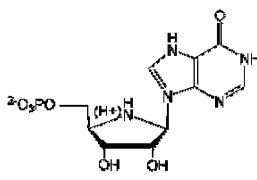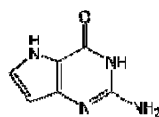
(9) Eads, J. C.; Scapin, G.; Xu, Y.; Grubmeyer, C.; Sacchettini, J. C. *Cell* **1994**, *78*, 325−334.
(10) Shi, W.; Li, C. M.; Tyler, P. C.; Furneaux, R. H.; Grubmeyer, C.; Schramm, V. L.; Almo, S. C. *Nat. Struct. Biol.* **1999**, *6*, 588−593.
(11) Balendiran, G. K.; Molina, J. A.; Xu, Y.; Torerres-Martinez, J.; Stevens, R.; Focia, P. J.; Eakin, A. E.; Sacchettini, J. C.; Craig, S. P., III. *Protein Sci.* **1998**, *8*, 1023−1031.
(12) Shi, W.; Li, C. M.; Tyler, P. C.; Furneaux, R. H.; Cahill, S. M.; Girvin, M. E.; Grubmeyer, C.; Schramm, V. L.; Almo, S. C. *Biochemistry* **1999**, *38*, 9872−9880.
(13) Héroux, A.; White, E. L.; Ross, L. J.; Kuzin, A. P.; Borhani, D. W. *Structure* **2000**, *8*, 1309−1318.
(14) Field, M. J. *A Practical Introduction to the Simulation of Molecular Systems*; Cambridge University Press: Cambridge, UK, 1999.
(15) Field, M. J.; Albe, M.; Bret, C.; Proust de Martin, F.; Thomas, A. *J. Comput. Chem.* **2000**, *21*, 1088−1100.
(16) *Jaguar_4.2*; Schrodinger Inc.: Portland OR.
(17) Dewar, M. J. S.; Zoebisch, E. G.; Healy, E. F.; Stewart, J. J. P. *J. Am. Chem. Soc.* **1985**, *107*, 3902−3909.
(18) Repasky, M. P.; Chandrasekar, J.; Jorgensen, W. L. *J. Comput. Chem.* **2002**, *23*, 1601−1622.
(19) Hehre, W. J.; Radom, L.; Schleyer, P. v. R.; Pople, J. A. *Ab Initio Molecular Orbital Theory*; Wiley & Sons: New York, 1986.
(20) Becke, A. D. *Phys. Rev. A* **1988**, *38*, 3098−3100.
(21) Jorgensen, W. L.; Maxwell, D. S.; Tirado-Rives, J. *J. Am. Chem. Soc.* **1996**, *118*, 11225−11236.
(22) Hutter, M. C.; J. M.; Reimers, J. R.; Hush, N. S. *J. Phys. Chem. B* **1999**, *102*, 8080−8090.
(23) Amara, P.; Field, M. J. *Theor. Chem. Acc.* **2003**, *109*, 43−52.
(24) Kumar, S.; Rosenberg, J. M.; Bouzida, D.; Swendsen, R. H.; Kolman, P. A. *J. Comput. Chem.* **1992**, *13*, 1011−1021.
(25) Roux, B. *Comput. Phys. Comm.* **1995**, *91*, 275−282.

Table 1. Details of the PRTase Crystal Structures Used in This Work[a]

PDB code	Specie	Resolution (Å)	Metal	Ligand 1	Ligand 2
1HMP[9]	Human	2.5	-	-	GMP
1BZY[10]	Human	2.0	$2Mg^{2+}$	PPi	ImmucillinGP
1D6N[11]	Human (K68A mutant)	2.7	$1Mg^{2+}$	PPi	7-hydroxy[4,3-d]pyrazolo pyrimidine
1CJB[12]	*Plasmodium falciparum*	2.0	$2Mg^{2+}$	PPi	ImmucillinHP
1FSG[13]	*Toxoplasma gondii*	1.05	$2Mg^{2+}$	PRPP	9-deazaguanine

[a] Listed for each structure are its PDB code and resolution, the species of origin, and cocrystallized active-site metals and ligands.

analyses were done on all stationary points, and visual inspection of the normal mode displacements was carried out with the VMD program.[26]

To ensure a reasonable sampling, 10−15 saddle point structures were obtained for the proton transfer (TS0) and phosphoribosyl transfer (TS1) steps in each protein (making ∼50 structures in all). Starting structures
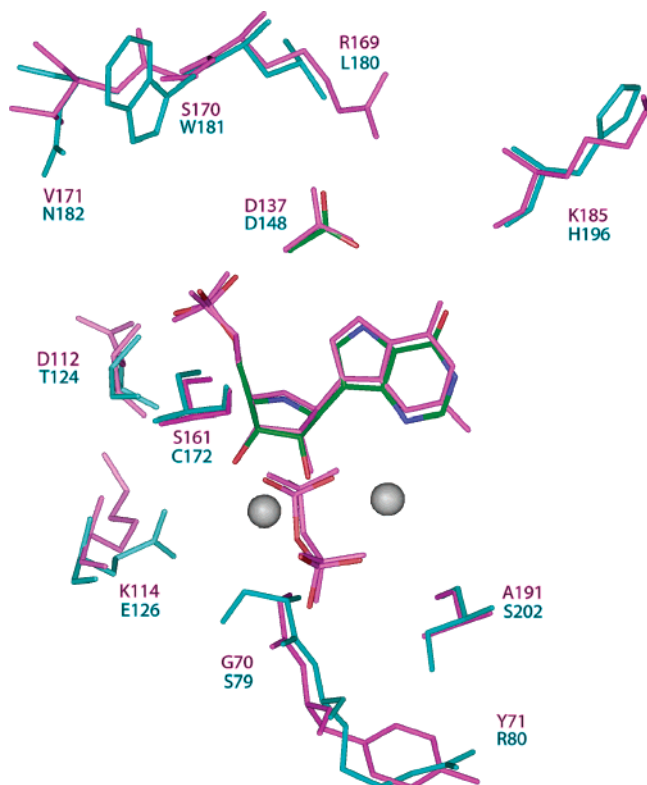
Figure 1. Superposition of the crystal structure active sites of human 1BZY (pink) and *Plasmodium falciparum* 1CJB (blue) HG(X)PRTases. Ligand atoms are colored according to atom type but only for the 1CJB structure. Also, for clarity, only the magnesium ions of the 1CJB site are shown (as gray spheres).

for the saddle-point searches were obtained by picking structures from the free-energy surface and performing constrained energy minimizations at appropriate values of ξ_1 and ξ_2.

To obtain ab initio corrected values for the reaction barriers, we generated reaction paths with the semiempirical hybrid potentials for the various reaction steps using constrained minimizations and then calculated energies for the reaction-path structures with both HF and DFT hybrid potentials.

To roughly estimate a correction, we took the "true" ab initio energy to be an average of the HF and DFT values. This followed from our previous work[27] in which we found that HF often overestimated barrier heights and DFT (with the B3LYP functional) often underestimated them. These average curves were then used to adjust the barrier heights of the semiempirical profiles.

Results

Remarkably, there was no qualitative and little quantitative differences between the mechanisms with hypoxanthine and xanthine in either enzyme. This indicates that the difference in specificity is not due to the chemical steps in the mechanism and lends support to the findings of the simulation study of Pitera et al. which suggested that the difference lay in the greater flexibility of the base-binding region of the *Pf* enzyme.[6]

The free energy surface for the human enzyme reaction with hypoxanthine as the base is illustrated in Figure 3. Our calculations indicated two feasible sequential mechanisms that are similar to those that we found previously for the *Pf* enzyme.[7,8] The first (blue dots) involves proton transfer of the H7 proton of the purine base to Asp137 to form an anionic

hypoxanthine intermediate, followed by phosphoribosyl transfer to form IMP. The second (green dots) involves phosphoribosyl transfer to form a cationic IMPH$^+$ intermediate, followed by loss of the H7 proton to the aspartate. A direct path (red dots) involving concerted phosphoribosyl and proton transfer is much higher in energy. In both the human and *Pf* enzymes, the phosphoribosyl transfer step is rate-limiting although the pathway via the anionic intermediate is preferred although the preference is less pronounced for the human enzyme. A direct path (red dots) involving concerted phosphoribosyl and proton transfer is much higher in energy.

In our previous study[7] we found that the structures and energetics calculated with the AM1 QM/MM potential compared well with those found using ab initio potentials but that the barrier height for the phosphoribosyl transfer step was overestimated. To obtain ab initio corrected barrier heights in this work, we generated optimized reaction paths for the phosphoribosyl transfer step with the AM1 hybrid potential and then performed point calculations at the ab initio HF and DFT levels of theory. An example is shown in Figure 4. Overall, we found that the barrier heights for the proton transfer steps in both enzymes were reasonably described by the AM1 potential but those for the phosphoribosyl transfer steps were overestimated by as much as 2-fold depending upon the path. The ab initio corrected free-energy values for the phosphoribosyl transfer step in both enzymes lie between 60 and 70 kJ mol^{-1} which is close to the experimental value.[5]

Although the barriers to phosphoribosyl transfer are similar in the human and *Pf* enzymes, the barrier to deprotonation in the human enzyme increases from ~30 to ~50 kJ mol^{-1}. An analysis of the interaction energies between the substrates and the enzymes for representative structures (see later) shows that this is due primarily to the replacement of Leu180 in the *Pf* enzyme by Arg169 in the human case. The latter hydrogen bonds to Asp137 and decreases its ability to extract the proton from the base. The essentially passive, structural roles of Arg169 and also of Lys165,[5] which hydrogen bonds to reactive atoms as well, were confirmed by simulations in which these residues were included in the QM region. No significant difference in the activation energy was observed with larger QM regions.

We also performed simulations to test the dependence of the mechanism on sugar conformation. In the *Toxoplasma gondii* 1FSG, *Pf* 1CJB and human 1BZY structures, the active site is reactant-like (complexed with transition-state analogues) and the ribose moiety has a C2′ endo conformation and O5′ is cis to O4′. In contrast, in the human 1HMP structure (complexed to GMP), the active site is product-like and the ribose sugar has a C2′ exo conformation and O5′ is trans to O4′. Simulations with both sugar conformations were performed. These showed that the sugar conformation can markedly affect the energetics of the reaction even though the preferred mechanism remains the same. A similar sensitivity of the energetics of a reaction to conformation has been observed by other workers.[28]

In our simulations, the preferred mechanism (by at least 20 kJ mol^{-1}) was one in which the ribose moiety in PRPP had a C2′ endo conformation and the O5′ atom was cis to the O4′

(26) Humphrey, W.; Dalke, A.; Schulten, K. *J. Mol. Graphics* **1996**, *14*, 33–38.

(27) Proust-De Martin, F.; Dumas, R.; Field, M. J. *J. Am. Chem. Soc.* **2000**, *122*, 7688–7697.
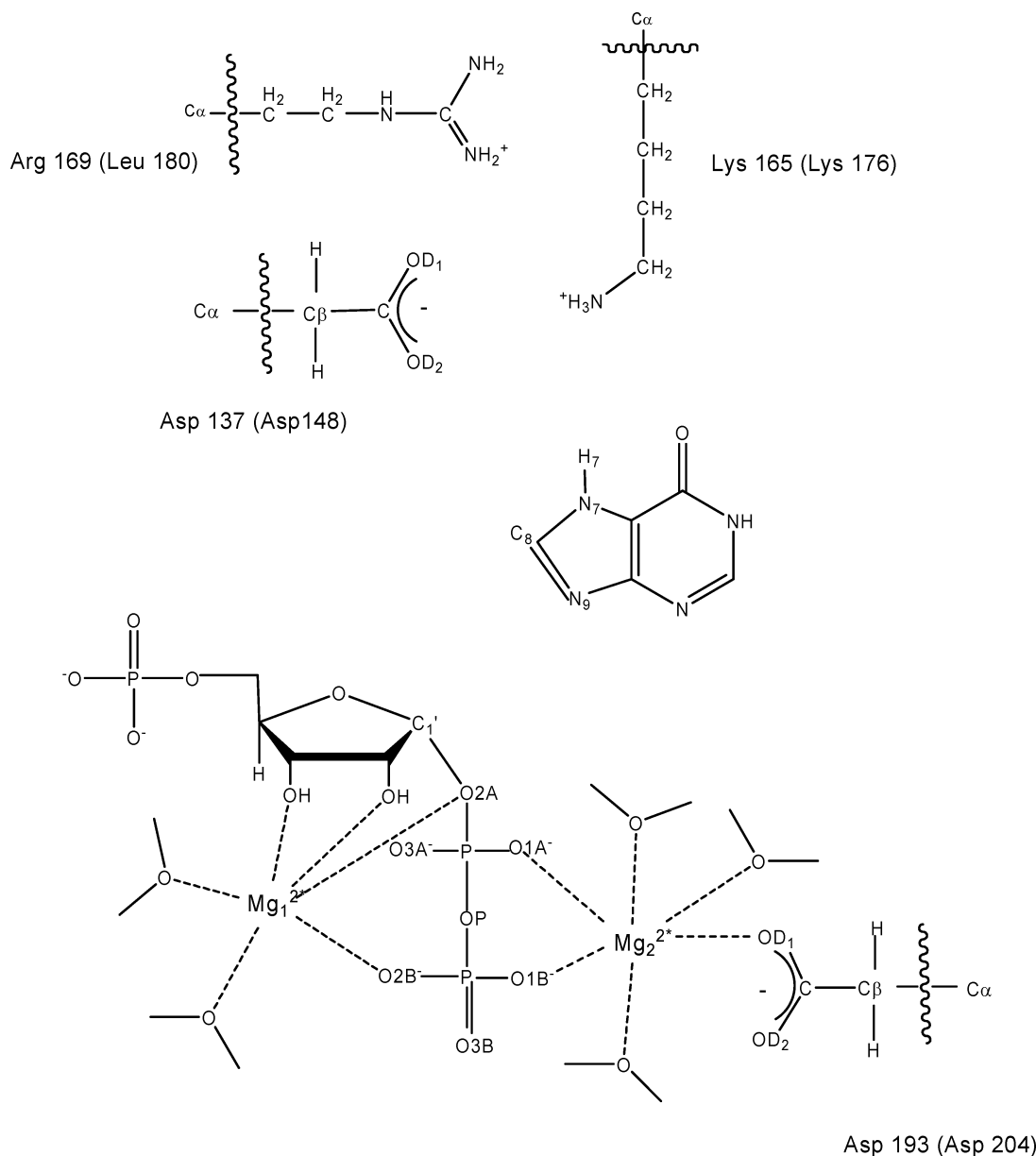
Figure 2. Schematic of the substrates and active-site residues in the human and *Pf* HG(X)PRTases included in the QM region of the hybrid potential simulations. *Pf* residue labels are given in parentheses.

atom. The conformation in C2′ exo is preferred for IMP, in agreement to what is seen in crystallographic experiments.

As a further probe of structural details along the reaction path, we used standard saddle-point location algorithms to characterize a number of TS structures for the deprotonation and phosphoribosyl transfer steps (denoted TS0 and TS1, respectively). Values of selected geometrical parameters for these TSs are given in Table 2.

The TSs for the deprotonation step in the human and *Pf* enzymes were very similar structurally despite the higher barrier in the human enzyme. In contrast, the TSs for the phosphoribosyl transfer step showed greater differences. The C1′−N9 distance of *Pf* TS1 resembles those of TSs identified experimentally in two other *N*-ribosyl transferases—bovine purine nucleoside phosphorylase (PNP)[29] and orotate PRTase[30]—that

have mechanisms of type D_NA_N. For these structures, the C1′−N9 distances are 1.77 and 1.85 Å, respectively, although the C1′−O2A distances are much longer at 3.0 and 3.8 Å, respectively. In contrast, the human enzyme has C1′−N9 distances similar to those of the ricin toxin-A chain[31] and to human and *Pf* PNPs.[32,33] These enzymes show dissociative mechanisms of type D_N*A_N with C1′−N9 distances of at least 3.0 Å.

Analyses of the interaction energies between the substrates and the surrounding active-site residues were performed using the standard pairwise energy decomposition scheme that is appropriate for semiempirical methods of the AM1 type but adapted for use with QM/MM potentials. The residue−ligand

(28) Garcia-Viloca, M.; Poulsen, T. D.; Truhlar, D. G.; Gao, J. *Protein Sci.* **2004**, *43*, 2341−2354.
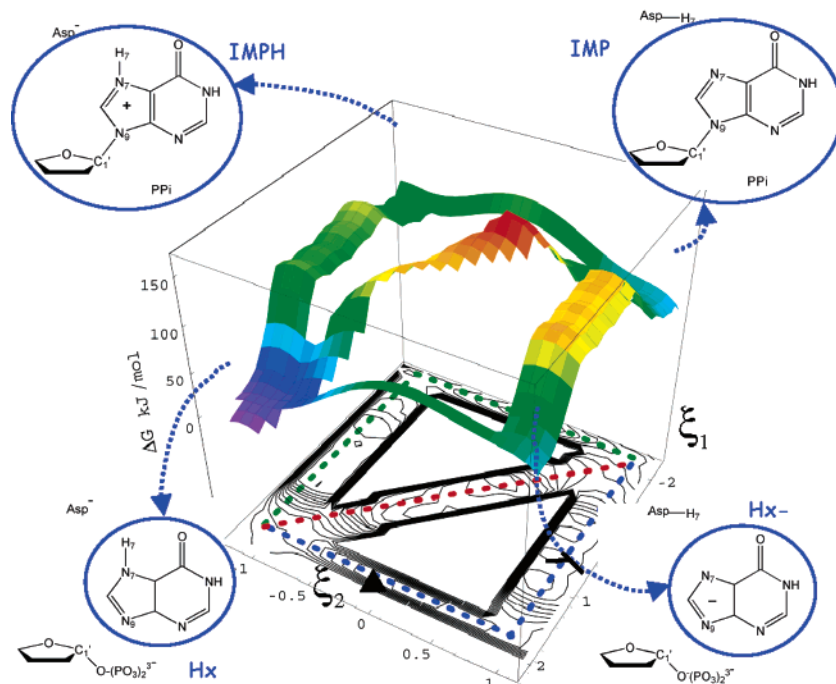(29) Kline, P. C.; Schramm, V. L. *Biochemistry* **1993**, *32*, 13212−13219.
(30) Tao, W.; Grubmeyer, C.; Blanchard, J. S. *Biochemistry* **1996**, *35*, 14−21.
(31) Chen, X.-Y.; Berti, P. J.; Schramm, V. L. *J. Am. Chem. Soc.* **2000**, *122*, 1609−1617.
(32) Lewandowicz, A.; Schramm, V. L. *Biochemistry* **2004**, *43*, 1458−1468.
(33) Shi, W.; Ting, L.-M.; Kicska, G. A.; Lewandowicz, A.; Tyler, P, C,; Evans, G. B.; Furneaux, R. H.; Kim, K.; Almo, S. C.; Schramm, V. L. *J. Biol. Chem,* **2004**, *279*, 18103−18106.

Figure 3. Free energy surface for the reaction of the human enzyme as a function of the reaction coordinates ξ_1 and ξ_2 which monitor phosphoribosyl and proton transfer, respectively. The black triangle and cross denote the TSs for the deprotonation and ribosyl transfer steps, respectively, along the preferred path.
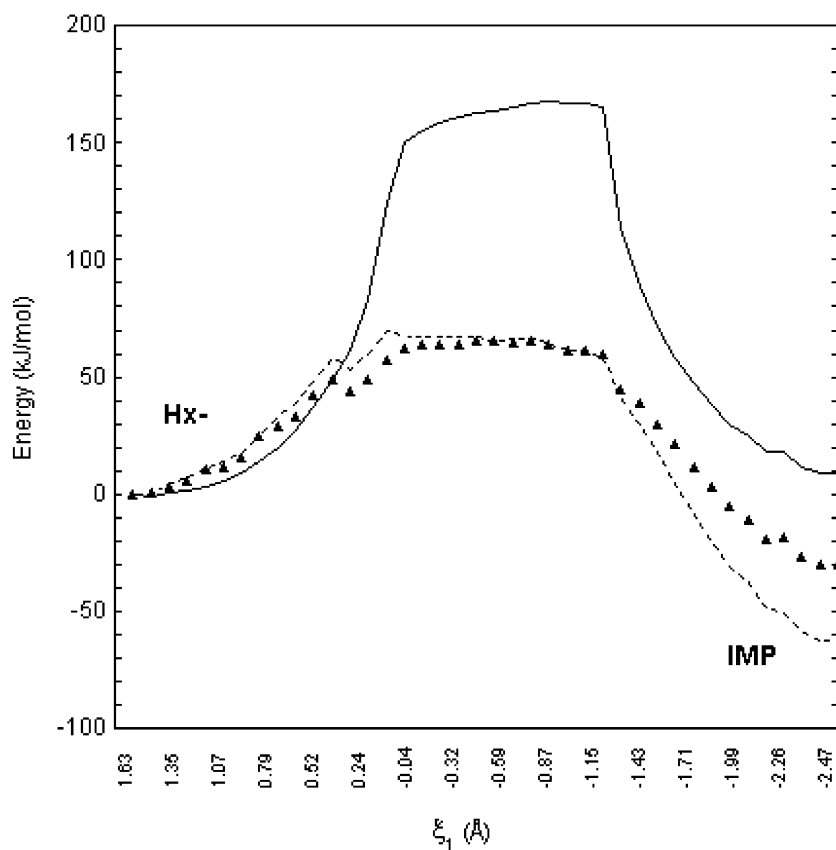

Figure 4. Sample energy curves for a reaction path describing the phosphoribosyl transfer step using AM1 (line), HF (dotted line), and DFT (triangles) hybrid potential methods. The path was optimized with the AM1 hybrid potential, and point calculations were performed at the ab initio levels of theory. All curves are shifted so that their energies are zero for the anionic intermediate.

interaction energies for selected human and *Pf* TS structures are shown in Figure 5.

There is much similarity in the interaction energies of the human and *Pf* enzymes, despite some residue differences be-

tween species. As noted previously, Arg169$_{hum}$ strongly stabilizes the human TSs in contrast to its *Pf* equivalent, Leu180$_{Pf}$. Another notable difference concerns two *Pf* residues, Arg112$_{Pf}$ and Lys151$_{Pf}$, that have interaction energies 2 to 3 times greater

Table 2. Means and Standard Deviations for Selected Geometrical Features of TS Structures from the Human and *Pf* Enzyme Reaction Mechanisms[a]

parameter	$TS0_{Pf}$	$TS0_{Hum}$	$TS1_{Hum}$	$TS1_{Pf}$
C1′−N9	3.30 ± 0.0005	3.06 ± 0.001	2.68 ± 0.08	1.90 ± 0.24
d(C1′−O2A)	1.42 ± 0.0004	1.43 ± 0.001	1.91 ± 0.22	2.34 ± 0.08
d(H7−N7)	1.22 ± 0.11	1.29 ± 0.17	1.82 ± 0.001	1.95 ± 0.002
d(H7−OD2)	1.32 ± 0.15	1.26 ± 0.14	1.01 ± 0.001	0.99 ± 0.001
angle(C4′−C3′−C2′−C1′)	-30.52 ± 0.03	-28.64 ± 0.11	-22.13 ± 0.88	-20.89 ± 2.08

[a] TS0 and TS1 correspond to the deprotonation and phosphoribosyl transfer steps, respectively. Distances are in Å, and the dihedral angle is in degrees.
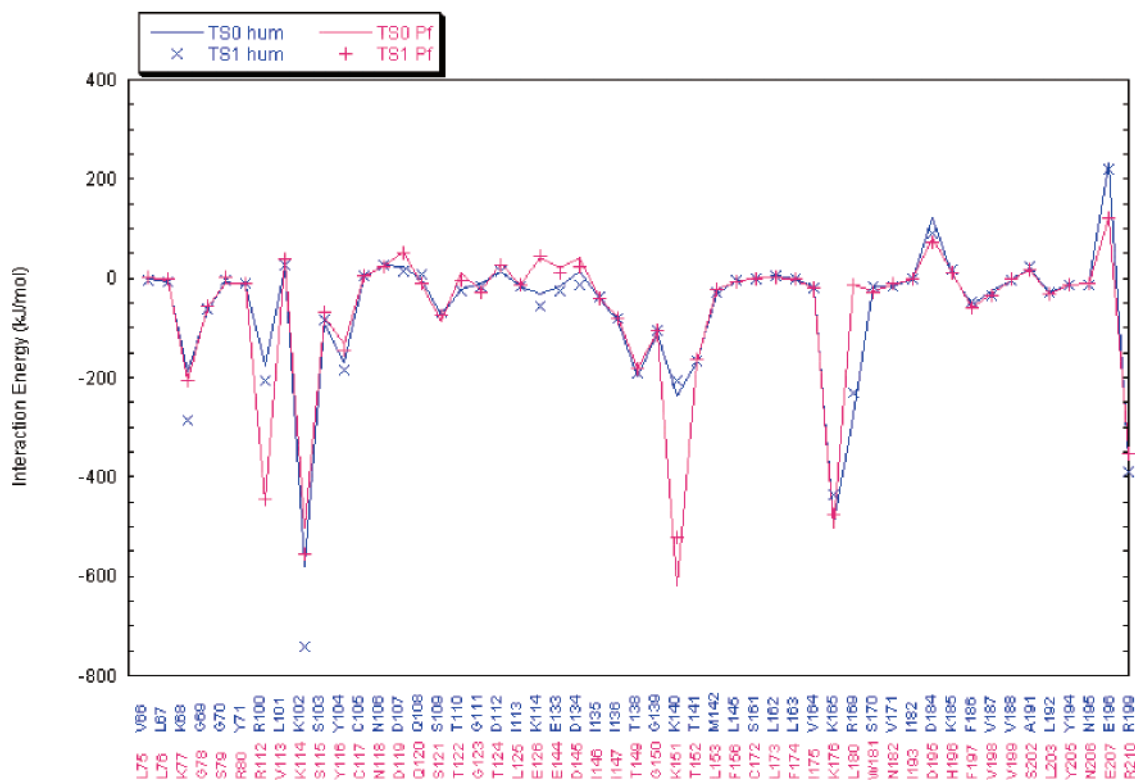
Figure 5. Residue−ligand interaction energies in the active sites of the human (pink) and *Pf* (blue) enzymes for selected examples of the TS0 and TS1 TS structures.

than those of their human counterparts, Arg100$_{hum}$ and Lys150$_{hum}$. This is because the latter residues in the human structure do not interact directly with the ligand but via water molecules.

Conclusion

In this paper, the reaction mechanisms of human HGPRTase and *Pf* HGXPRTase have been simulated. This a complement to our previous work on the *Pf* enzyme.[7,8] In both enzymes, the preferred path is one in which deprotonation of the base occurs first followed by phosphoribosyl transfer. The ab initio corrected barrier height for the phosphoribosyl transfer step is close to the experimentally determined one.[5] TS structures for each step have also been characterized using saddle-point location and normal-mode calculations. The *Pf* phosphoribosyl transfer TS was characterized as being of type $D_N A_N$, because the breaking sugar−PPi bond is short compared to the distance between the attacking nucleophile and sugar. The equivalent human TS structure attests of a slightly different mechanism, as the base and sugar are at van der Waals distance, whereas the leaving group is further away. It is significant that the TS structures for the human and *Pf* HG(X)PRTases differ as they do (by 0.8 Å in the C1′−N9 interatomic distance) given that their energetics are so similar.

Previous experimental work on PNPs[34] has shown that small structural differences of the order of ∼0.4 Å in some interatomic distances can be important for the design of inhibitors that target specific enzymes. Likewise, it is to be hoped that the differences observed here, if confirmed, can be exploited for the conception of potential therapeutic molecules that selectively inhibit the *Pf* enzyme.

(34) Schramm, V. L. *Arch. Biochem. Biophys.* **2005**, *433*, 13−26.